Progress Report for the Period July 1991 to December 1991

NASA LaRC Grant No. NAG-1-1215:

Improvements to a Method for the Geometrically Nonlinear Analysis of Compressively Loaded Stiffened Composite Panels

This report describes progress made during the period July 1991 to December 1991 on the tasks identified in the technical proposals for the subject grant. The plans for further effort on each of the tasks are outlined. The computer implementation of the method of analysis under development is referred to in this document as NLPAN.

i) Implementation of Continuation Methods

In the progress report for the preceding period of performance [1], an outline was given of the theory behind the implementation of two so-called "continuation methods," namely Riks' method [2] and Thurston's method [3], within the NLPAN computer code. The methods are used for traversing limit points and bifurcation points, respectively, in the equilibrium load/response behavior of stiffened panels. Problems were encountered in the present reporting period which led to some changes both to the implementation of the two continuation methods, and to the fundamental formulation used in NLPAN, as described in Ref. [4]. These problems and changes are briefly described here. Complete details of the modified theory are included in a theory document which is under preparation, and which will be released during the next period of performance.

The set of nonlinear algebraic equations which are ultimately solved in order to compute equilibrium solutions are written symbolically as

$$f_i(\bar{q}, \lambda) = 0 \ , \quad i = 1, 2, \ldots, M \tag{2}$$

where lambda is the generalized load parameter, and q_i is the i^{th} modal amplitude, $i = 1, 2, \ldots, M$. The following two matrices play roles in the two continuation methods

$$D_{ij}^{o} = \frac{\partial f_i(\bar{q}, \lambda)}{\partial q_j}$$

$$D_{ij}^{\delta} = \frac{\partial^2 f_i(\bar{q}, \lambda)}{\partial q_j \partial \lambda} \tag{3}$$

and in Ref. [1] it was stated that the tangent stiffness matrix, $[D^o]$, is symmetric, and that the negative matrix $[-D^{\delta}]$ is both symmetric and positive definite. Both of these assumptions have been found to be false. If a function f_i is derived from a total potential energy function, π, by the relationship

$$f_i = \frac{\partial \pi}{\partial q_i} \tag{4}$$

then the corresponding tangent stiffness defined by equation (2) will indeed be positive definite [2]. It was thus discovered that the virtual work approach behind NLPAN as described in [4] does not, as was previously believed, correspond to a statement of stationary total potential energy.

Because of the desire to have a symmetric tangent stiffness matrix for the sake of the solution procedures for the nonlinear algebraic equations, the direct application of the principle of virtual work was abandoned and replaced with an approach which begins with a total potential energy expression. The new approach has led to certain restrictions regarding the selection of load control versus displacement control for the in-plane loads on a panel, and these restrictions are summarized in Table 1.

The assumption that the matrix $[-D^{\delta}]$ is symmetric and positive-definite was fundamental to the approach described in Ref. [1] for monitoring the stability of the equilibrium state, and because the assumption was incorrect, a change was required. The eigenvalue problem posed in [1],

$$([D^o] + \omega_k[D^{\delta}])\{\phi^k\} = \{0\} \ , \quad k = 1, 2, \ldots, M \tag{5}$$

has been replaced with by the following eigenvalue problem:

$$([D^o] - \omega_k[I])\{\phi^k\} = \{0\} \ , \quad k = 1, 2, \ldots, M \tag{6}$$

where [I] is the identity matrix. This eigenvalue problem is used to determine the stability of an equilibrium solution; when the equilibrium path approaches a critical stability state, the lowest eigenvalue, ω_1, goes to zero.

Results computed using both Riks' method and Thurston's method are presented in Figure 1. The configuration modelled is a rectangular isotropic plate with bi-axial loading applied through control of the in-plane normal displacements at each edge. Other aspects of the plate configuration are given in the figure. Two-mode analyses were performed for the purpose of illustrating the operation of the two methods discussed here. First, a perfect plate was modelled, and Thurston's method was used for navigating past the three bifurcation points, labeled A, B, and C, which are encountered along the equilibrium path, labeled Path 1. Next, an imperfect plate was modeled, where the imperfection shape has contributions in the shapes of both of the mode shapes used. The equilibrium path of the imperfect plate, labeled Path 2, exhibits two limit points, labeled D and E, and these limit points were traversed in the analysis using Riks' method. Both of the curves were generated by the same automated computer procedure which integrates the two continuation methods. There are two dots on each equilibrium path. One dot on each path indicates where the equilibrium state of the plate becomes unstable for a load steadily increased from zero, and the other dot on each path indicates the state at which an actual plate would come to rest after a dynamic snap.

One difficulty with the two solution methods discussed here is that for some configurations, the second eigenvalue of equation (6) goes to zero, indicating, it is believed, that there are multiple unstable equilibrium paths which intersect. No robust logic for tracking through such a tangle has been established, and NLPAN has been programmed to terminate the solution process when this situation is encountered. The dynamic analysis discussed below is designed to circumvent this complication.

ii) Dynamic Analysis Capability

The purpose of the dynamic analysis capability is to analytically locate the stable equilibrium state sought by a structure which has passed from a stable equilibrium state to an

unstable one, and which thus begins a transient dynamic response. It is assumed that the dynamic response occurs at a fixed value of the generalized load, namely the value at which the equilibrium solution becomes unstable, and that damping is present to dissipate energy. The detailed formulation of the dynamic analysis is provided in a theory document which will be released during the next reporting period. A brief summary of the approach is given here.

The form of the nonlinear algebraic equations governing equilibrium is given by

$$(\lambda C_i^L + C_i^o) + q_j(\lambda C_{ij}^L + C_{ij}^o) + q_j q_k(\lambda C_{ijk}^L + C_{ijk}^o) + q_j q_k q_\ell(\lambda C_{ijk\ell}^L + C_{ijk\ell}^o) = 0 \ , \quad i = 1, 2. \ldots, M \tag{7}$$

where summation is implied over repeated indices, λ is the generalized load parameter, and the M modal amplitudes, q_i $(i = 1, 2, \ldots, M)$, are the generalized coordinates of the structure. The above equations represent the condition of stationary total potential energy. Hamilton's principle is applied in order to obtain the equations of motion, and an equation of the following form is ultimately obtained:

$$\ddot{q}_j C_{ij} + \dot{q}_j \dot{C}_{ij} + q_j C_{ij} + q_j q_k C_{ijk} + q_j q_k q_\ell + C_{ijk\ell} = 0 \ , \quad i = 1, 2. \ldots, M \tag{8}$$

where $\dot{q}_i$ and $\ddot{q}_i$ are the first and second time derivatives, respectively, of the j^{th} modal amplitude, and where

$$\begin{aligned} C_i &= \lambda^* C_i^L + C_i^o & \qquad C_{ijk} &= \lambda^* C_{ijk}^L + C_{ijk}^o \\ C_{ij} &= \lambda^* C_{ij}^L + C_{ij}^o & \qquad C_{ijk\ell} &= \lambda^* C_{ijk\ell}^L + C_{ijk\ell}^o \end{aligned} \tag{9}$$

where λ^* is the value of the generalized load parameter at the critical equilibrium state, and

$$\dot{C}_{ij} = \sum_{p=1}^{P} \left(\sum_A \mu w_i w_j \, dA \right)_p \tag{10a}$$

$$\ddot{C}_{ij} = \sum_{p=1}^{P} \left(\sum_A m(v_i v_j + w_i w_j) \, dA \right)_p \tag{10b}$$

where p is a plate strip index number, P is the total number of plate strips in the structure, μ is a viscous damping coefficient with units of force per unit area, per unit velocity, m is the mass per unit area of a plate strip, and v_i and w_i are components of the buckling modes.

The Newmark direct integration procedure [5] will be used to solve equations (8) at a series of uniform time steps. Because the goal of the analysis is to locate a new equilibrium solution, the selection of the viscous damping coefficient and the time increment need not be made with the concern of obtaining exact or realistic dynamical solutions. Nonetheless, the selection of the two parameters mentioned will effect the performance of the dynamic solution strategy. The basis for the selection of the parameters has not yet been established, but the issue will be taken up when coding of the dynamic analysis procedure is complete.

iii) Additional Boundary Condition Options for the Panel Ends

The formulation has been completed for two new varieties of boundary conditions which can be imposed at the longitudinal ends of a panel, namely clamped ends, and eccentrically applied end loading. For the clamped-end case, the condition which is sought is that the axial displacement is the same for all points at each end of the panel. Because this condition can not generally be satisfied exactly, the error in the satisfaction of the boundary condition is minimized in the least squares sense. This is accomplished through the use of the penalty function method [6].

In modelling load eccentricity, the goal is to simulate a line across the end section of the panel along which the load is assumed to be applied in the fashion of a knife-edge. The modelling of this support condition is more complicated than for the clamped-end simulation. Several points in the panel cross-section are specified which define the line of load application. These points are constrained to move together using the penalty parameter method, and an additional variable parameter is added to the expression of displacements. The new parameter controls an end-shortening correction to the first-order displacements, in order to provide the condition that the pivoting (due to the first-order displacements) of the panel ends about the eccentric load lines occurs without any effective change in the end-shortening value.

Coding of the method for modelling the two different end-support conditions mentioned above in in progress, and the details of the formulation are in a theory document to be released in the next reporting period. An additional task planned is to develop and implement in NLPAN the ability to model elastic restraint at the panel ends.

iv) Transverse Pressure Loading

As described in the previous progress report, the ability to model transverse pressure loading has been developed and encoded in the NLPAN computer program. Further progress during the present reporting period has been the implementation of a method for controlling asynchronous application of the in-plane loading and the transverse pressure loading. Denoting the in-plane load parameter as λ and the pressure load parameter as β, a series of target load pairs, $(\lambda_o, \beta_o) = (0,0)$, (λ_1, β_1), (λ_2, β_2), ... is specified which bound a series of load ranges. In each load range, parameters λ and β vary linearly with a new, generalized load parameter, ζ, where ζ varies from zero to one within each load interval. Thus, the two load parameters are replaced with a single one, and the solution strategies for the nonlinear algebraic equations can be readily applied. It is noted that the in-plane load parameter, λ, may control either in-plane normal loads or in-plane normal displacements, consistent with the selections made from Table 1. The details of the theory for transverse pressure loading and the method of controlling asynchronous loading are contained in a theory document to be released in the next period of performance.

As an example of the application of asynchronous loading, NLPAN was used to model a long isotropic plate subjected to combined axial compression and transverse pressure. The configuration is one for which results were computed by Levy et al [7], and details of the configuration are provided in Figure 2a). For verification purposes, four buckling mode shapes were incorporated in the NLPAN analysis corresponding to the four double sine functions used in the Ref [7] to represent out-of-plane displacements. The computed values of axial load versus end-shortening are presented in Figure 2b), and it can be seen that there is essentially exact agreement between the NLPAN predictions and the results of Ref. [7]. The NLPAN analysis was conducted using two load intervals, the first of which corresponded to the ap-

plication of transverse pressure with zero net end load. It can be seen that the panel shortens in length due to the application of the transverse pressure. The second interval simulates the application of axial loading while the transverse pressure maintained at a constant value. Rik's method was called on by the NLPAN analysis in order to traverse the multiple limit points which are encountered. During the next period of performance, NLPAN will be used to model stiffened panel configurations subjected to pressure loading.

v) Second-Order Displacement Fields

As discussed in the previous progress report, there is a discrepancy in the functional form of the second-order displacement fields with regard to satisfaction of the boundary conditions at the longitudinal ends of a panel. The transverse displacement components of the buckling modes, v_i and w_i, vary as $\sin(m\pi x/L)$ in the longitudinal direction, where m is the integer halfwave number, and thus these displacement components go to zero at the longitudinal ends of a panel. In contrast, the transverse displacements of the second-order displacement fields, v_{ij} and w_{ij}, vary as $\cos(\hat{m}\pi x/L)$ in the longitudinal direction, where $\hat{m}$ is an integer, and thus v_{ij} and w_{ij} do not in general go to zero at the panel ends.

Recent efforts toward addressing this problem have focused on the fact that the ordinary differential equations governing the y-dependence of the second-order displacement functions are identical to the ordinary differential equations which govern the y-dependence of the buckling eigenfunctions, with the distinction that the latter differential equations are homogeneous, whereas the former equations are not, and where it is understood that the two sets of ordinary differential equations referred to depend on the the associated halfwave number, $\hat{m}$ or m, respectively. The similarity of the two sets of differential equations has several implications. First, the second-order displacement fields contain contributions which correspond to buckling mode shapes, except that the phase difference with respect to the longitudinal direction causes the points of maximum displacement to occur at the ends of the panel, where they violate the boundary conditions. Second, the degree to which particular buckling mode shapes are present in a second-order displacement field depends on the reference value of the load parameter used in computing the second-order field. The shape of the field is thus

highly dependent of the reference load level selected, and amplitude of the field becomes unbounded when the reference load level coincides with a buckling eigenvalue for the particular halfwave number associated with the field being computed.

It would seem that the ideally, the second-order fields should be forced to be orthogonal to all buckling mode shapes, in which case the second-order displacement fields would truly be second-order in nature in that they would not duplicate displacement contributions which could be represented by the inclusion of buckling mode shapes in the analysis. It is suspected that the second-order fields would then be both load-independent, and would be much more in accordance with the boundary conditions at the panel ends. In analyses of thin-walled structural sections, Benito and Sridharan [8] enforced orthogonality of the second-order displacement fields with respect to the buckling modes through the use of the Lagrange multiplier method. This approach has the disadvantage of eliminating the banded quality of the coefficient matrix of the linear system of equations which is solved to obtain a discrete representation of a second-order field by the current method. Thus, enforcing the orthogonality condition by this method may add significantly to the computational cost. This and other means of enforcing the will be investigated further during the next period of performance.

vi) Additional Tasks

Additional efforts are planned in the next reporting period, consistent with the continuation proposal recently submitted to NASA Langley Research Center. The most significant of these tasks is to develop the ability within NLPAN to model the effects of thermal loading. An additional task is to improve the computational economy of NLPAN, both with respect to central processing unit execution times, and with respect to computer core memory requirements. Reductions in the core memory requirements will result in an increase in the modelling accuracy available, because of the ability to incorporate a larger number of mode shapes in an analysis. Finally, an attempt will be made to automate the process of selecting the mode shapes to be incorporated in an NLPAN analysis. Currently, this selection is left to the discretion of the program user, but systematic approaches have been developed for selecting

mode sets for certain types of configurations, and it is planned to implement these approaches in an automated fashion.

vii) Results for an I-Stiffened Panel with a Complex Cross-Section

NLPAN was used to model the postbuckled response of a stiffened graphite/epoxy panel with a complicated cross section, which called for the use of offsets between the plate strip edges and their associated node lines. The ability of NLPAN to account for these offsets has not previously been exercised. The configuration modelled is a stiffened panel for which experimental results are given by Starnes et al [9]. The panel has four stiffeners, and was flat-end tested in uniaxial loading. Some details of the panel configuration are given in Figure 3a-b), and complete details are given in Ref. [9]. A unit cell representation was used in the NLPAN analysis, and a schematic drawing of the cross-section of the unit cell is shown in Figure 3c). The unit cell model employed 17 plate strips and 12 node lines, and a three-step representation of the tapered flanges of the test article was used. The node-line offsets referred to above are visible in Figure 3c. Symmetry conditions were enforced at the side-edges of the unit cell. A four-mode NLPAN analysis was used, where the dominant mode was the primary local-buckling mode having five halfwaves along the length of the panel, and the three additional mode shapes were selected based on their ability to provide the refinement of the displacement field (with respect to the primary buckling mode shape) which takes place in postbuckling. An initial imperfection was used in the NLPAN model in the shape of the primary buckling mode and having an amplitude of one percent of the panel skin thickness.

Results for end load versus end shortening are presented in Figure 4a), and the agreement between the NLPAN predictions and the experimental results is fairly good, though NLPAN predicts slightly less axial stiffness in postbuckling than was observed experimentally. (The NLPAN model used the unsupported length of the panel for the postbuckling analysis, with a correction added to account for the compression of the panel ends within the potted ends.) The distribution of longitudinal membrane strains (in the panel skin) across the width of the center bay at the mid-length of the panel are shown for three different load levels in Figure 4b). The agreement between the theory and the experiment is good except for a slight

over-prediction of strain levels by NLPAN near the center of the panel at the higher load levels.

In Figure 5, results are presented for longitudinal strains on opposing surfaces at two locations on the mid-length of the panel, as affected by the panel loading. Figure 5a) shows the location of strain gages used to obtain the experimental results. The strain levels at the center of the panel skin are plotted in Figure 5b), and the agreement between the experiment and theoretical results is fairly good. NLPAN over-predicts the strain amplitudes slightly at the higher load levels, and this is consistent with the discrepancy noted regarding the results of Figure 4b). The strain levels at a stiffener flange location are plotted in Figure 5c). The strains predicted by NLPAN run uniformly about 10% less than the reported experimental values. There was some disagreement between the slopes of the curves in prebuckling, so the experimental results were plotted a second time with the strain values scaled down so that the prebuckling slopes of the theory and experiment match; the modified experimental curves lie nearly on top of the theoretically curves. The reason for the discrepancy in the prebuckling slopes is not apparent, but the qualitative agreement between the theoretical results and the experimental results provides some confidence that the node-line offset feature of the NLPAN program is working properly.

References

1. Stoll, F., "Progress Report for the Period January 1991 to June 1991, NASA LaRC Grant No. NAG-1-1215: Improvements to a Method for the Geometrically Nonlinear Analysis of Compressively Loaded Stiffened Composite Panels," submitted to the NASA Scientific and Technical Information Facility, Baltimore, Maryland, June, 1991.

2. Riks, E., "An Incremental Approach to the Solution of Snapping and Buckling Problems," *Int. J. Solids and Structures*, Vol. 15, 1979, pp. 529-551.

3. Thurston, G.A., "Modal Interaction in Postbuckled Plates: Theory," NASA TP-2943, November, 1989.

4. Stoll, F., "A Method for the Geometrically Nonlinear Analysis of Compressively Loaded Prismatic Composite Structures," PhD dissertation, Department of Engineering Science and Mechanics, Virginia Polytechnic Institute and State University, Blacksburg, Virginia, January 1991.

5. Reddy, J.N., *An Introduction to the Finite Element Method*, McGraw-Hill Book Company, New York, 1984, pp. 54-56.

6. Reddy, J.N., *Energy and Variational Methods in Applied Mechanics*, John Wiley and Sons, New York, 1984, Section 2.2.

7. Levy, S., Goldenburg, D., and Zibritosky, G., "Simply Supported Long Rectangular Plates Under Combined Axial Load and Normal Pressure," NACA TN 949, 1944.

8. Benito, R., and Sridharan, S., "Interactive Buckling Analysis with Finite Strips," *Int. J. for Numerical Methods in Engineering*, Vol. 21, 1985, pp. 145-161.

9. Starnes, J.H. Jr., Knight, N.F. Jr., and Rouse, M., "Postbuckled Behavior of Selected Flat Stiffened Graphite-Epoxy Panels Loaded in Compression," *AIAA Journal*, Vol. 23, No. 8, August, 1985, pp. 1236-1246.

Load Case	Flat Skin?	In-Plane Loading Characteristics	Control Param.: *L*- Edge Load *D*- Edge Displ.	B.C. Option for Component 2 in Table 2.
A	Yes	Constant Ratio: $N_{y_G} : N_{x_G}$ 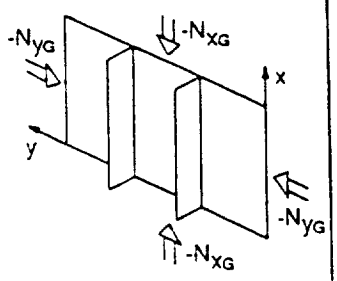	*L* / *D* if $N_{yG} = 0$ *L* if $N_{yG} \neq 0$	2/3
B	Yes	$\Delta v = 0$ 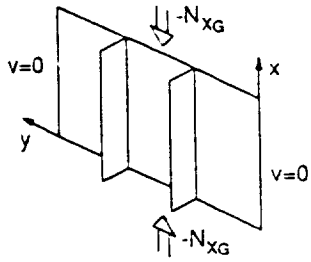	*L* / *D*	1
C	Yes	Constant Ratio: $\Delta v : \Delta u$ 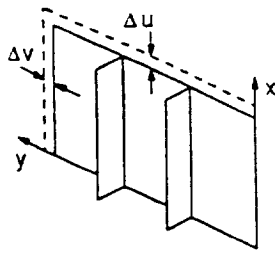	*D*	1
D	No	Nominal Uniaxial Loading 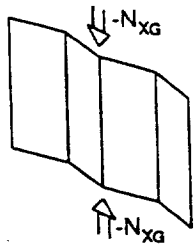	*L* / *D*	1/2/3

Table 1. Options for Controlling the In-Plane Loading.

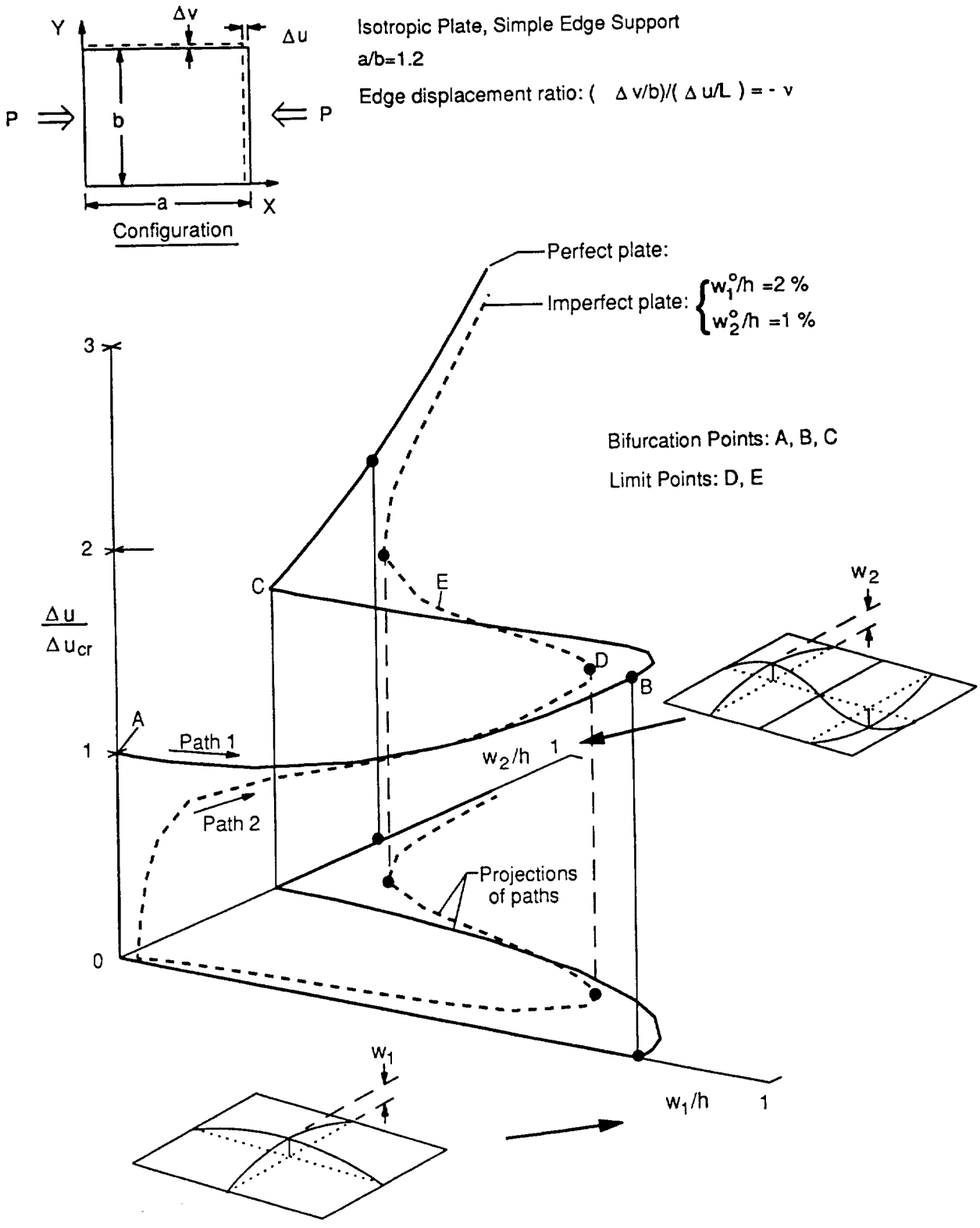

Figure 1. Equilibrium solutions computed using Riks' method and Thurston's method.

a/b=4

Simple support on all edges

All edges constrained to remain straight

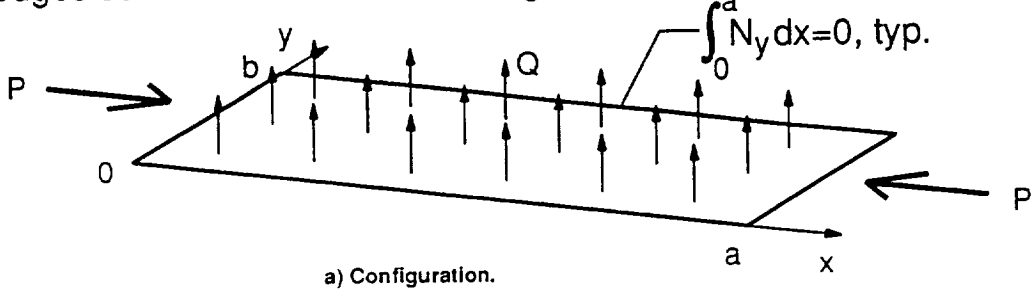

a) Configuration.

Assumed form for w(x,y):

$$w(x,y)=[w_{11}\sin(1\,\pi\,x/a)+w_{31}\sin(3\,\pi\,x/a)+w_{51}\sin(5\,\pi\,x/a)+w_{71}\sin(7\,\pi\,x/a)]\sin(\pi\,y/b)$$

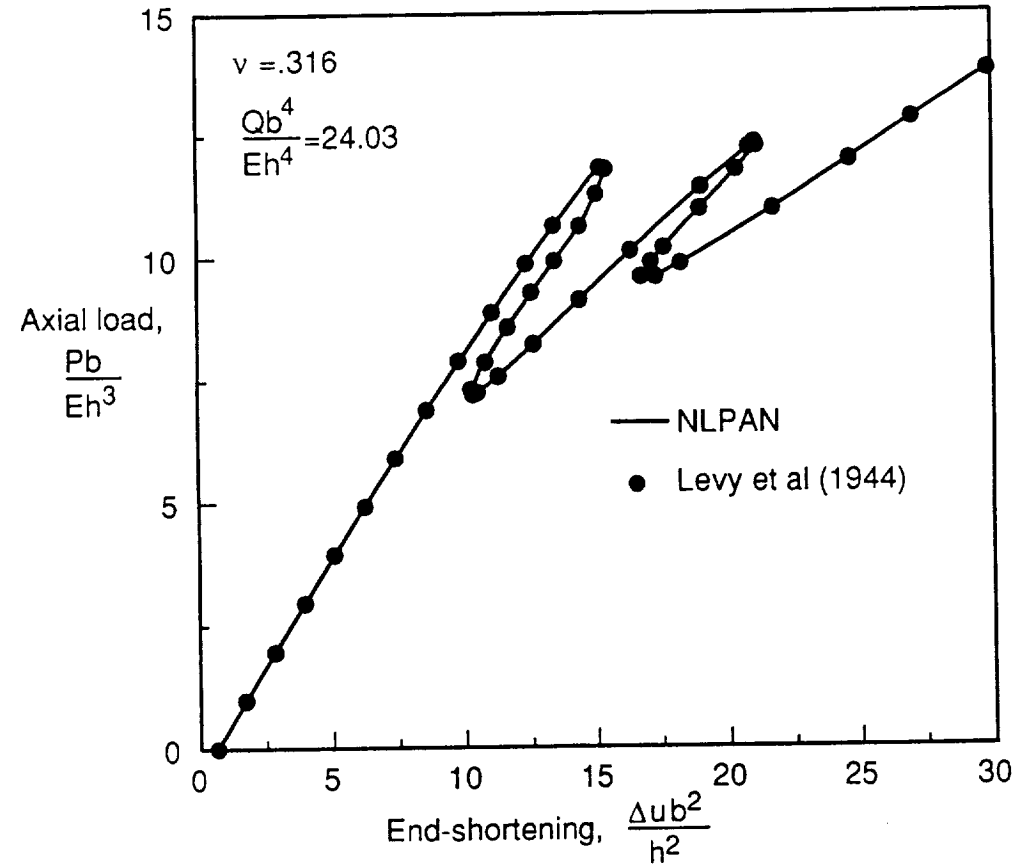

b) Axial load versus end-shortening.

Figure 2. Isotropic rectangular plate under combined axial and pressure loading.

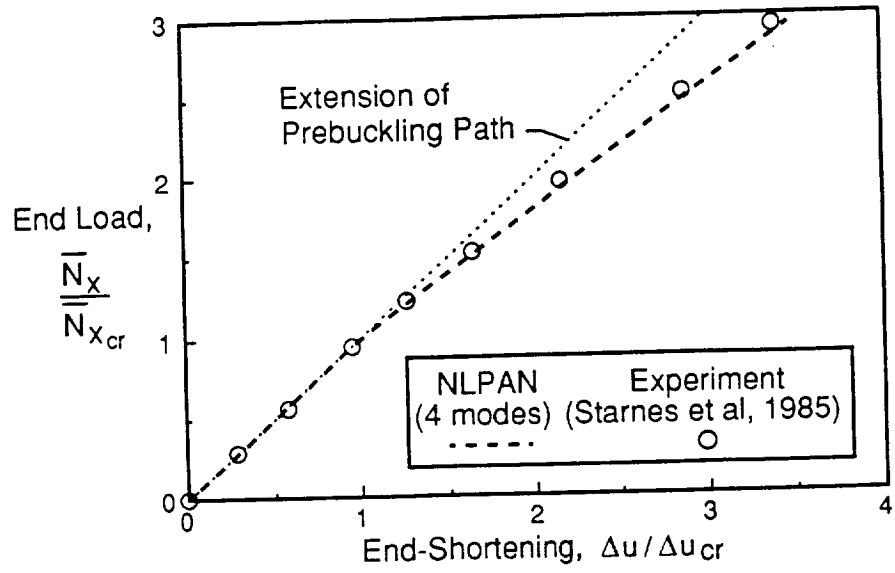

a) End load versus end-shortening.

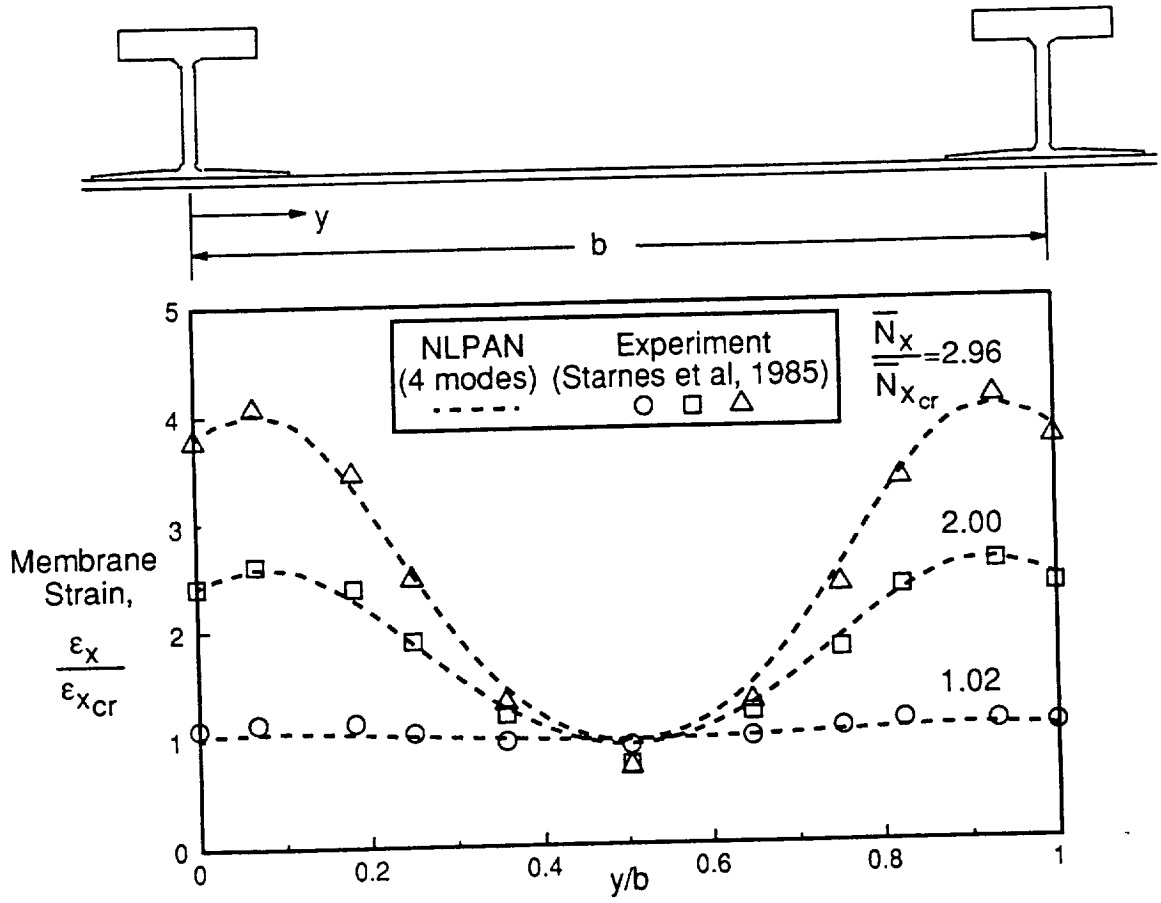

b) Membrane strains in the skin, mid-length, center bay.

Figure 4. Analytical and experimental results for a stiffened graphite/epoxy panel in postbuckling.

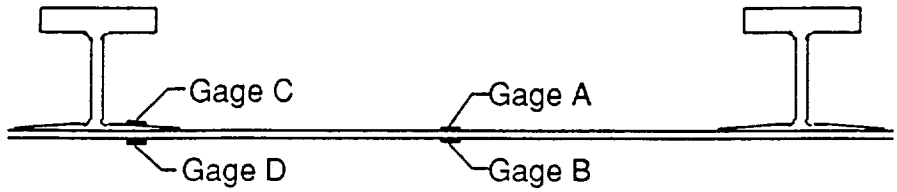

a) Strain gage placement at the mid-length of the center bay.

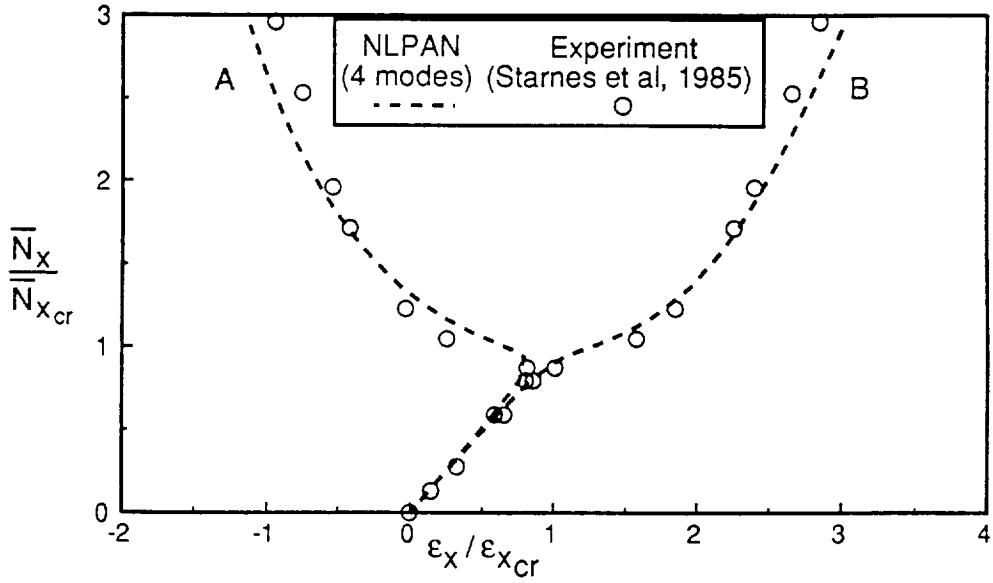

b) Strains at the center of the skin.

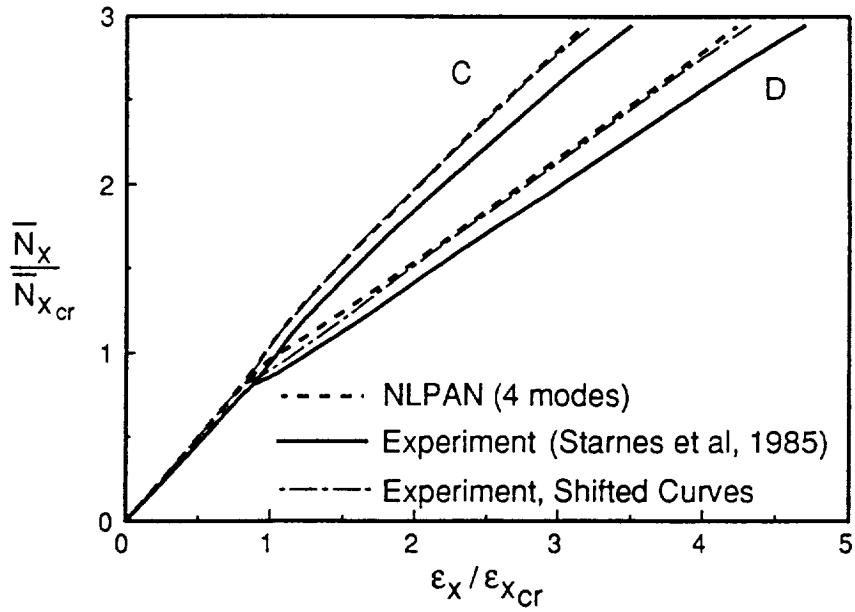

c) Strains at the stiffener flange.

Figure 5. Longitudinal surface strains on a stiffened graphite/epoxy panel in postbuckling.